

## **Abstract**

Urban areas experience numerous environmental challenges, among which the anthropogenic emissions of heat and carbon are two major contributors, the former is responsible for the notorious urban heat effect, the latter longterm climate changes. Moreover, the exchange of heat and carbon dioxide are closely interlinked in the built environment, and can form positive feedback loops that accelerate the degradation of urban environmental quality. Among a handful countermeasures for heat and carbon mitigation, urban irrigation is believed to be effective in cooling, yet the understanding of its impact on the co-evolution of heat and carbon emission remains obscure. In this study, we conducted multiphysics urban climate modeling for all urban areas in the contiguous United States, and evaluated the irrigation-induced cooling and carbon mitigation. Furthermore, we assessed the impact of urban irrigation on the potential heat-carbon feedback loop, with their strength of coupling quantified by an advanced causal inference method using the convergent cross mapping algorithms. It is found that the impact of urban irrigation varies vastly in geographically different cities, with its local and non-local effect unraveling distinct pathways of heat-carbon feedback mechanism.

**Keywords:** *Causality; Contiguous United States; Convergent cross mapping; Heat-carbon feedback; Irrigation; Urban microclimate*

## 1. Introduction

Urban areas accommodate 56% of the world population (UN, 2019), but cover only about 3% of Earth's land surface (Lambin and Meyfroidt, 2011; Gao and O'Neill, 2020). Cities, especially the larger ones, are the hotspots of burgeoning human activities, also known as the "anthropogenic stressors" (Fernando, 2010), which has been the primary and the most irreversible driver to climate changes (Seto et al., 2011; IPCC, 2022). The concentrated anthropogenic stressors in urban areas, alongside the irreversible modification of land use and land cover, give rise to drastic environmental consequences, including the exacerbated thermal environment, air pollution, infrastructure vulnerability, public health risks, and degraded ecosystem services, to name a few (Antognelli & Vizzari, 2016; USGCRP, 2016; Kumar et al., 2019; Demetillo et al., 2020; Wang, 2021).

Among anthropogenic stressors, heat and carbon dioxide (CO<sub>2</sub>) emissions are the two primary sources. Urban areas today consume over two thirds of world's energy, and produce about 70% of global carbon emissions (UN-Habitat, 2020). Anthropogenic heat emissions, together with other contributors including the presence of urban morphology, reduced vegetation coverage, and the use of engineering materials, are mainly responsible for the exacerbated thermal environment in urban areas. One prominent example is the well-known phenomenon of urban heat island (UHI) effect, viz. urban cores can be significantly warmer than their rural surroundings (Oke, 1967, 1982; Wang, 2022). Large cities, with their densely populated residential areas and infrastructure, particularly fall prey to the exacerbated thermal environment over the last few decades (Habeeb et al., 2015).

In addition, most sources of anthropogenic heat emissions, such as vehicles and industrial buildings, are also significant contributors of greenhouse gas (GHG) emissions, especially the

anthropogenic carbon dioxide (AnCO<sub>2</sub>) (Pataki et al., 2006; Hutyra et al., 2011). On the global scale, AnCO<sub>2</sub> emissions constitute the largest carbon flux to the atmosphere and represent the dominant source of GHG forcing to climate changes (Gurney, 2014). The increase of CO<sub>2</sub> concentration produces rising global mean temperature, which, in turn, results in higher AnCO<sub>2</sub> emissions by, e.g., more fossil fuel burning in buildings and vehicles, leading to a positive loop and vicious cycle of *climate-carbon feedback* in the Earth's climate system (Randerson et al., 2015), via land-atmosphere interactions over built terrains (Song & Wang, 2015, 2016; Song et al., 2017).

Last decades have witnessed the burgeoning interest and tremendous effort of researchers, policymakers, and practitioners, devoted to seeking sustainable countermeasures to anthropogenic emissions for ameliorating the urban environmental quality, in particular, on heat mitigation strategies and carbon-neutral cities (Wang et al., 2021; Huovila et al., 2022). Among these countermeasures, urban irrigation has been extensively studied as an effective means for reducing the ambient temperature while supporting the biogenic functions of urban vegetations (Yang and Wang, 2015; Luketich et al., 2019; Wang et al., 2019). Its impact on the dynamic of carbon exchange in urban areas has been hitherto relatively underexplored but starts to attract more research endeavor lately (Hardiman et al., 2017; Sargent et al. 2018; Li and Wang, 2021a, 2021b; Li et al., 2022). Nevertheless, the compound effect of urban irrigation on the co-evolution of heat and carbon exchange in the built environment remains largely obscure, especially on altering the possible pathways of heat-carbon feedback mechanisms.

In local environments, e.g., street canyons, where urban irrigation takes place, it can modify the heat-carbon interactions in two major, but competing, processes. First, by effective cooling of the built environment, controlled urban irrigation can suppress biogenic and AnCO<sub>2</sub>

emission via, say reduced use of electricity or fossil burning for air conditioning in buildings and cars, hence achieve the environmental co-benefit of heat and carbon mitigation (Li et al., 2021). On the contrary, irrigation of urban vegetation can lead to an increase of abiotic carbon emission, mainly through soil respiration (Decina et al., 2016; Kindler et al., 2022). In the long run, these irrigation-induced changes in local environment will also surface in spatially adjacent or even distant areas (de Vrese et al., 2016), via the long-range connectivity of urban areas (aka teleconnection) (Seto et al., 2012) that leads to “analog” in thermal environment even among cities far apart from one another (Fitzpatrick and Dunn, 2019).

Given the inadequacy of *status quo* understanding of the intriguing yet complicated temperature-CO<sub>2</sub> interactions, we aim to disentangle and unravel the physics of coupled heat and carbon exchange in urban areas. Given the time series of a pair of environmental variables, say temperature and abiotic carbon emission, prevailing practices to determine their coupling strength is through the measure of statistical correlation, such as Pearson’s  $r$ . Nevertheless, statistical correlation, fitful for linear systems, is inadequate to capture the true coupling of variables in nonlinear dynamics such as the urban climate system. For example, *spurious* correlations between a pair of variables are commonly found, even in simple nonlinear systems (Myerud et al., 2001). Therefore, to determine the true heat-carbon coupling and its strength, causal inference, instead of statistical correlation should be used (Pearl and Mackenzie, 2018; Runge et al., 2019). In this study, we adopt an advanced causal inference approach, namely the convergent cross mapping (CCM) algorithm (Sugihara et al., 2012), to quantify the local and non-local impact of urban irrigation on the potential heat-carbon feedback loops. The CCM method is particularly fitful for detecting causal relations in nonlinear and moderately coupled dynamic systems (e.g. climate systems).

The rest of the paper is organized as follows. The methods used in this study are described in Section 2, including the study areas, regional hydroclimate modeling, urban land surface processes, and the CCM method for quantification of true coupling links and their strength. It is followed by results of hydroclimate modeling and causal analysis in Section 3, accompanied by discussions in the light of new findings. We then conclude the study with remarks on the major findings and their implications, together with caveats and perspectives to future study.

## 2. Methods

In this study, our study area consists of all urban areas in the contiguous United States (CONUS) with densely developed land and over 50,000 or more population, according to the Topologically Integrated Geographic Encoding and Referencing (TIGER) Geodatabase developed by U.S. Census Bureau (<https://www.census.gov/geographies/mapping-files/time-series/geo/tiger-geodatabase-file.html>). The spatial distribution of the classified urban pixels is shown in **Fig. 1a**, based on the National Land Cover Database (NLCD) Landsat imagery with 30-m resolution (Wickham et al., 2014), and the corresponding fractions of built-up areas.

### 2.1. WRF simulations of urban climate

We used the mesoscale Weather Research and Forecasting (WRF) model (v4.0) for the urban climate simulations of CONUS cities (Skamarock et al., 2019). WRF is a fully compressible, Euler nonhydrostatic numerical weather prediction and atmospheric simulation system, which has been widely used at multiple spatiotemporal scales. An important feature of ARW is that it includes the enhanced land surface parameterizations of Noah-MP (Niu et al., 2011), including vegetation canopy dynamics, multi-layer soil and snowpack with liquid water

retention, and frozen ground physics. In this study, we configured the spatial domain of to cover the entire CONUS and its surrounding regions in Canada and Mexico, with a 5-km grid size in horizontal directions and 32 vertical layers. The use of parameterization schemes for different dynamic solvers including planetary boundary-layer and surface-layer dynamics, cloud microphysics, and short- and long-wave radiation followed the choice in Wang et al. (2019a).

Moreover, the land surface processes in non-urban areas were simulated using the unified Noah land surface model (Noah-LSM), while dynamics of surface exchange in urban cells were modeled using the single layer urban canopy model (UCM). Three urban categories were adopted in the WRF model, viz. low-residential, high-residential, and commercial areas, respectively, each with the UCM input defined in WRF urban parameter table correspondingly (Wang & Upreti, 2019). In addition, a “tiling approach” was used to reflect the surface heterogeneity as well as to calculate the meteorological condition, such as temperature, aggregated over urban and non-urban portion within a given gridcell (Chen et al., 2011). We also chose nudging options based on previous studies (Wang et al., 2018, 2019a, 2019b) for evaluating different urban strategies over the same study area, viz. CONUS cities, at various spatiotemporal resolutions.

## 2.2. Carbon exchange in the built environment

In this study, we adopted a state-of-the-art urban land surface model, viz. the Arizona Single Layer Urban canopy Model (ASLUM) (Wang et al., 2013) to capture the CO<sub>2</sub> exchange in the built environment, subjected to the local microclimate conditions generated by the mesoscale WRF model. The latest version of ASLUM (v.4.0) (Li and Wang, 2020; Wang et al., 2021) features a holistic set of parameterization schemes for urban CO<sub>2</sub> uptake and emission

arising from various sources, including human, building, and vehicular CO<sub>2</sub> emissions, plant biogenic CO<sub>2</sub> fluxes, and ecosystem respiration, via a data fusion approach. The biogenic CO<sub>2</sub> exchange, including CO<sub>2</sub> exchange from urban green spaces, is parameterized to resolve the interplay between physical environment and biochemical processes. In particular, the gross primary production (GPP) is given by,

$$\text{GPP} = f_V \int_0^{LAI} F_{GPP}(PAR, T_{sk}, [CO_2], \theta) dL, \quad (1)$$

where  $f_V$  is the vegetation fraction;  $F_{GPP}$  is the  $A_g-r_s$ -type plant photosynthesis model adopted in ASLUM;  $LAI$  is the leaf area index;  $PAR$  is the photosynthetically activated radiation;  $T_{sk}$  is the leaf skin temperature;  $[CO_2]$  is near surface CO<sub>2</sub> concentration level in ppm; and  $\theta$  is the normalized soil moisture (saturation). The special integral sums leaf level carbon assimilation rate to canopy level primary production when considering the light extinction inside of the canopy (Ronda et al., 2001). In addition, the in-canyon soil respiration  $R$  is calculated as,

$$R = f_S F_R(T_s, \theta, LAI), \quad (2)$$

where  $f_S$  is the soil fraction;  $F_R$  is the temperature-dependent respiration function; and  $T_s$  is top-soil layer temperature. The net ecosystem exchange (NEE) is then calculated as  $NEE = R - GPP$ , with both  $R$  and  $GPP$  being the magnitude (both positive) of carbon exchange rate. The directions of NEE follow the sign convention used in ecological studies with negative values designating net carbon absorption by vegetation, *vice versa*.

### 2.3. Convergent cross mapping for causal inference

In this study, to quantify the heat-carbon coupling/feedback strength, we adopt the CCM method for causal inference between the time series of temperature and a given carbon flux, at either the same town (local causality) or different urban areas (non-local impact). To apply the

CCM algorithms, the aggregated mean values at each time instant of the 24-hour cycle are subtracted from the original time series. Thus, only the detrended time series of anomalies are used for subsequent causality analysis. The purpose of the detrending process is to remove the impact of periodicity, viz. the diurnal cycle, intrinsic to temperature and carbon dynamics that are subject to a common external forcing, viz. solar radiation, and susceptible to produce spurious causality.

The CCM algorithm for causal inference has been developed for detecting the directed causal influence in moderately-coupled nonlinear dynamic systems, such as Earth's climate system. The method is based on the classic delay-coordinate embedding theory for nonlinear time series analysis (Takens, 1981), with a nearest-neighbors algorithm for reconstruction of the cross-mapping estimate (Sugihara and May, 1990; Sugihara et al., 2012). The fundamental idea of the CCM algorithm is that if causality exists between a pair of generic variables, represented by two time series  $X(t)$  and  $Y(t)$  respectively, then the cross-mapping dynamics of one variable can be reconstructed from the information of the other, and *vice versa*. To quantify the causal inference from  $Y$  to  $X$ , it starts by constructing a shadow manifold  $M_X$  from  $X(t)$  by re-arranging the original time series into a lagged-coordinate vector, denoted as  $\mathbf{x}(t) = [X(t), X(t-\tau), \dots, X(t-(E-1)\tau)]$ , where  $\tau$  and  $E$  are the time delay and embedding dimension, respectively. It follows that cross-mapping estimates can then be constructed from the manifolds. For example, the cross-mapping  $\hat{Y}(t) | M_X$  can be constructed using a simple projection of the  $E+1$  nearest neighbors of vector  $\mathbf{x}(t)$  in the manifold of  $M_X$ , with exponentially weighted distances.

Lastly, the causality from  $Y$  to  $X$  is measured by the correlation coefficient  $\rho_{Y|M_X}$  between the original  $Y(t)$  and the cross-mapping estimate  $\hat{Y}(t) | M_X$ , given by

$$\rho_{Y|M_X} = \frac{\mathbf{E}\left\{\left[Y(t) - \mu_Y\right] \cdot \left[\hat{Y}(t) | M_X - \mu_{\hat{Y}}\right]\right\}}{\sigma_Y \sigma_{\hat{Y}}}, \quad (3)$$

where  $\mathbf{E}$ ,  $\mu$ , and  $\sigma$  are the statistical expectation, average, and standard deviation, respectively. A larger value  $\rho_{Y|M_X}$  implies a stronger casual influence, while  $Y$  is not causal to  $X$  if  $\rho_{Y|M_X} \leq 0$ .

Likewise, the causality from  $X$  to  $Y$  can be quantified using the aforementioned procedure by constructing the cross-mapping estimate  $\hat{X}(t) | M_Y$  and finding its correlation to the original data series of  $X(t)$ . In addition, the accuracy of the CCM algorithm can be sensitive to the choice of the time delay  $\tau$  and the embedding dimension  $E$ . Both parameters for the time series of similar nature, say temperatures, can be determined using the correlation integral and dimension method (Grassberger and Procaccia, 1983; Lai and Ye, 2003). In this study, we adopted  $\tau = 1$  and  $E = 3$  following our previous analysis for temperature series (Yang et al. 2022, 2023).

### 3. Results and Discussion

#### 3.1. The impact of urban irrigation on mitigating heat and carbon emissions

We first evaluated the model performance of WRF simulations by comparing the predicted 2-m air temperature in CONUS urban areas against field measurements from the Global Historical Climatology Network (GHCN) database. The results of comparisons are shown in **Fig. 1**. It can be seen that the model results are in good agreement with measurement with a root-mean-square-error (RMSE) of 2.14 °C, which is within the usual range of uncertainty of WRF temperature predictions.

We then conducted urban climate simulations using WRF over the summer of four months, from 01 May to 30 August, in 2013, under controlled experiments without (the “baseline” scenario) and with urban irrigation (the “irrigated” scenario). A standard daily irrigation scheme

during 21:00 to 22:00 local time was applied uniformly throughout all urban areas, which stopped once the soil water content reaches the field capacity, following the guideline of typical practice of municipal irrigation (Gober et al., 2010). The output of WRF simulation was calculated at a timestep of 30 second, including surface level temperatures, air pressure, humidity, incoming solar radiation, soil moisture, etc. These variables were then aggregated at an hourly interval for model outputs.

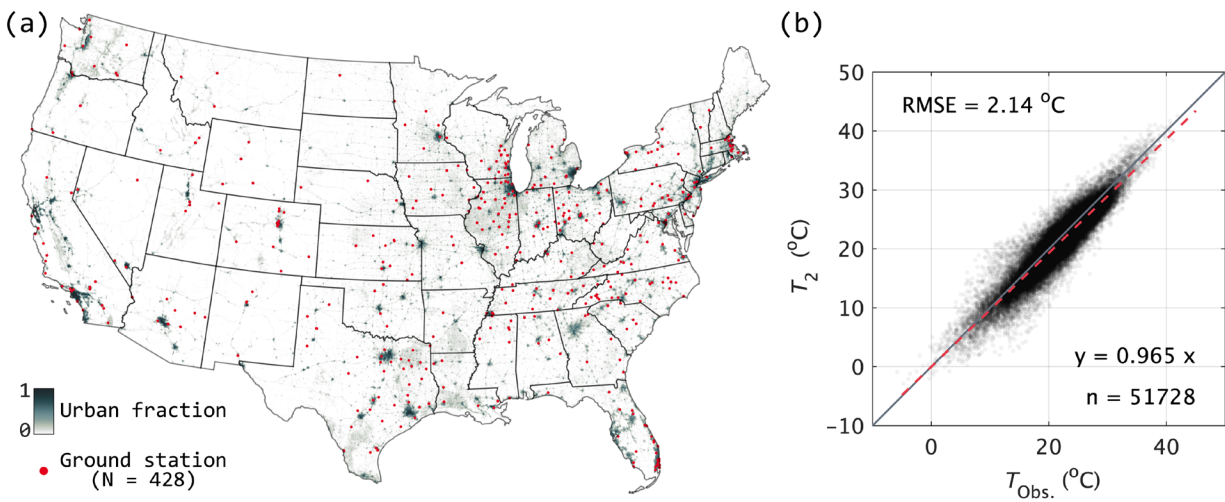


**Figure 1.** (a) Urban fraction over CONUS and GHCN ground stations used in this study for temperature validation; (b) comparison between WRF simulated daily mean 2-meter temperature ( $T_2$ ) and daily mean air temperature from GHCN stations ( $T_{obs.}$ ). Dashed red line represents the linear regression of scattered data points ( $n = 51728$ ).

The results of the changes, i.e. the difference between the irrigated and baseline scenarios, of the *magnitude* of the 2-m temperature  $dT_2$ , and that of the surface  $CO_2$  fluxes, viz.  $dGPP$ ,  $dR$ , and  $dNEE$  are mapped into each urban gridcell in CONUS, as shown in Figure 2. Urban irrigation improves the thermal environment with a ubiquitous reduction of the near-surface temperature in all urban areas (**Fig. 2a**). The cooling effect varies spatially with, in general, the

most significant impact on densely populated urban clusters, e.g. metropolitans in the Northeast corridor, the Great Lake area, Florida, Texas, California, and Arizona.

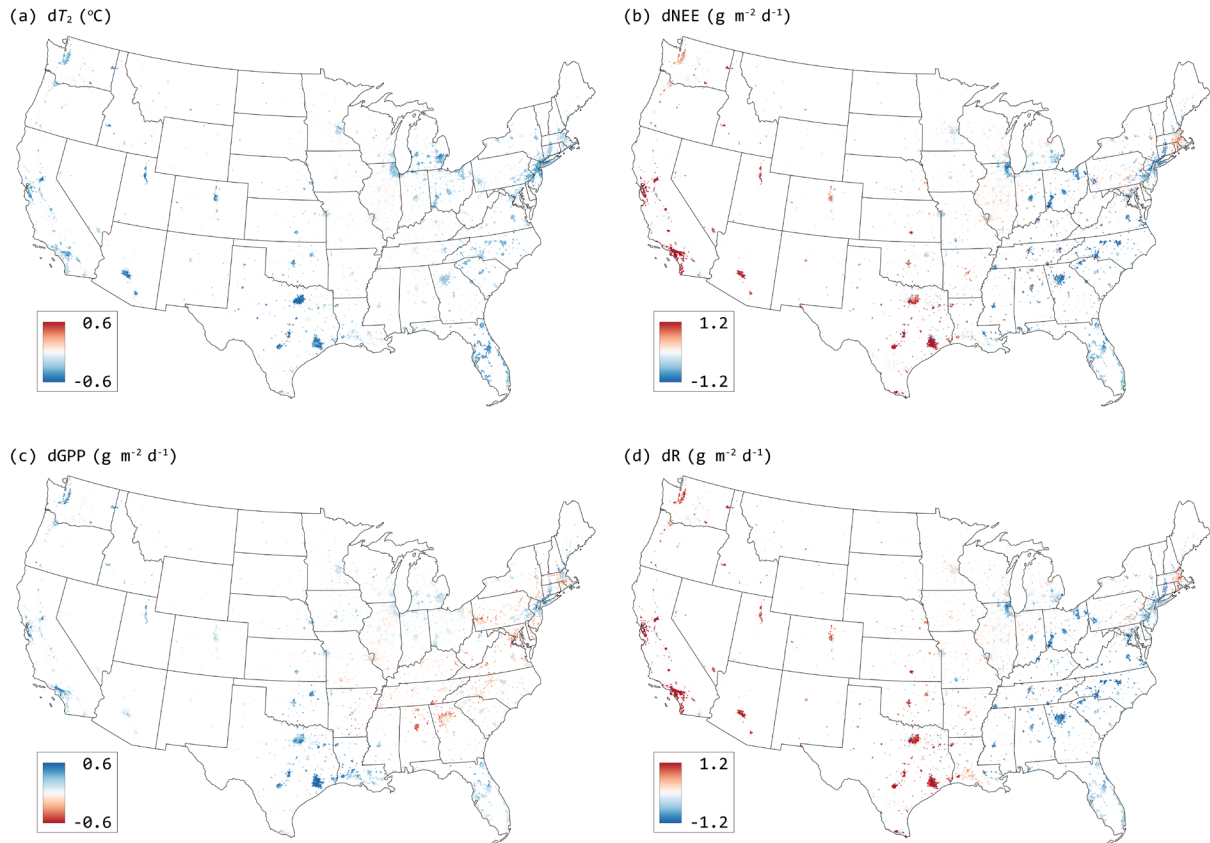


**Figure 2.** Change of temperature and carbon fluxes due to urban irrigation in (a) 2-m temperature  $dT_2$ , (b) net ecosystem exchange  $dNEE$ , (c) gross primary production  $dGPP$ , and (d) soil respiration  $dR$ . The color bars are designed such that the cool (blue) spectrum shows desirable results with urban irrigation (reduced temperature and carbon emissions), whereas the warm (red) spectrum shows adverse effect.

The impact of urban irrigation on individual carbon exchange processes is more complex and intriguing. The response of carbon exchange to irrigation in CONUS urban areas, on the other hand, exhibits two rather distinct regions, roughly representing the east and west halves of

CONUS, where the opposite effect can be found in irrigation-induced carbon emissions. For example, in the regions east to Great Lakes and Ohio Valley, there is a significant reduction of soil respiration  $dR$  (blue areas in **Fig. 2d**), indicating the effect is favorable as carbon mitigation, whereas the change is generally unfavorable in the west with vast areas of arid/semiarid regions. Or in other words, urban irrigation induces a net environmental co-benefit of heat-carbon (in terms of  $R$ ) mitigation in east CONUS, but a clear trade-off between cooling and enhanced soil respiration in the west, both were mechanistically investigated and reported in our previous study (Li and Wang, 2021a). In particular, the urban irrigation-induced increase in soil respiration in the west is consistent with the finding in a lately reported site measurement using a mobile eddy-covariance tower located in the Phoenix metropolitan areas (Kindler et al. 2022).

The impact of urban irrigation on GPP shows an opposite spatial distribution over CONUS, as compared to that on  $R$ , i.e. it is generally unfavorable (decrease in GPP) in the east CONUS (demarcated by red urban pixels), but favorable in the west (**Fig. 2c**). This implies that urban irrigation, while enhancing soil respiration (e.g. in the west), also promotes carbon assimilation by plants via photosynthesis. The magnitude of  $dGPP$ , however, is often smaller than that of  $dR$ , presumably because the effect of irrigation on the microbial process in soil (via soil respiration) is more direct and stronger than that in the atmosphere (via photosynthesis). This difference leads to the overall impact of irrigation on NEE is dominated by the change of respiration (**Fig. 2b**), as revealed by the striking similarity in their patterns of spatial distribution (c.f. **Fig. 2d**).

### 3.2. CCM causality in comparison with statistical correlation

After obtaining the dataset of WRF model outcome on urban temperature and carbon fluxes, we then proceed to quantify their *strength of coupling*, a strong indicator to potential

heat-carbon feedback mechanism. We first tested the proposed causality algorithm, viz. the CCM method, in comparison to the prevailing linear statistical correlation. To do this, we used the WRF-predicted time series of  $T_2$ , GPP, NEE and R in a selected urban area of CONUS, viz. Phoenix city, shown in **Fig. 3a**, and detrended the diurnal cycles to yield the corresponding anomalies (**Fig. 3b**). The results of linear correlation and CCM causality matrices are shown in **Fig. 3c** and **Fig. 3d**, respectively. In these matrices, we removed the self-correlation or causality, represented by the diagonal entities in **Figs. 3c&d**, and concentrated the off-diagonal terms.

It is noteworthy that the correlation matrix is symmetrical, but the directional causality matrix is asymmetrical, *by definition*, as the causal influence e.g. by near-surface temperature  $T_2$  on soil respiration R is not necessarily the same as R on  $T_2$ , while the statistical correlation between the two time series always remains the same without directionality. Moreover, we found that the CCM method is capable of capturing the strong causal influence of  $T_2$  on all the carbon fluxes (the first row in **Fig. 3d**), whereas their statistical correlations are rather mild or even weak (the first row in **Fig. 3c**). On the other hand,  $T_2$  is weakly susceptible to all surface carbon fluxes either statistically or causally (c.f. the first columns in **Fig. 3c** and **Fig. 3d**), even more so in terms of causality. This finding shed the first new light on the true heat-carbon coupling (and feedback) in that the causal relationship is capable of not only discovering the spurious correlation, but also manifesting the mechanistically significant (true) interactions.

In addition, among the three carbon fluxes, NEE is causally linked to both R and GPP (as per definition, NEE is the sum of the two), but the causality is strong between NEE and R, which is consistent with the results and interpretation of the WRF outcome in **Fig. 2**. There is no causal relationship between GPP and R, as they are governed by independent physical processes, while there exists some weak to moderate degree of statistical correlation, which is likely due to their

response to common forcing in the nonlinear urban climate system, and can be regarded as spurious in the light of CCM results.

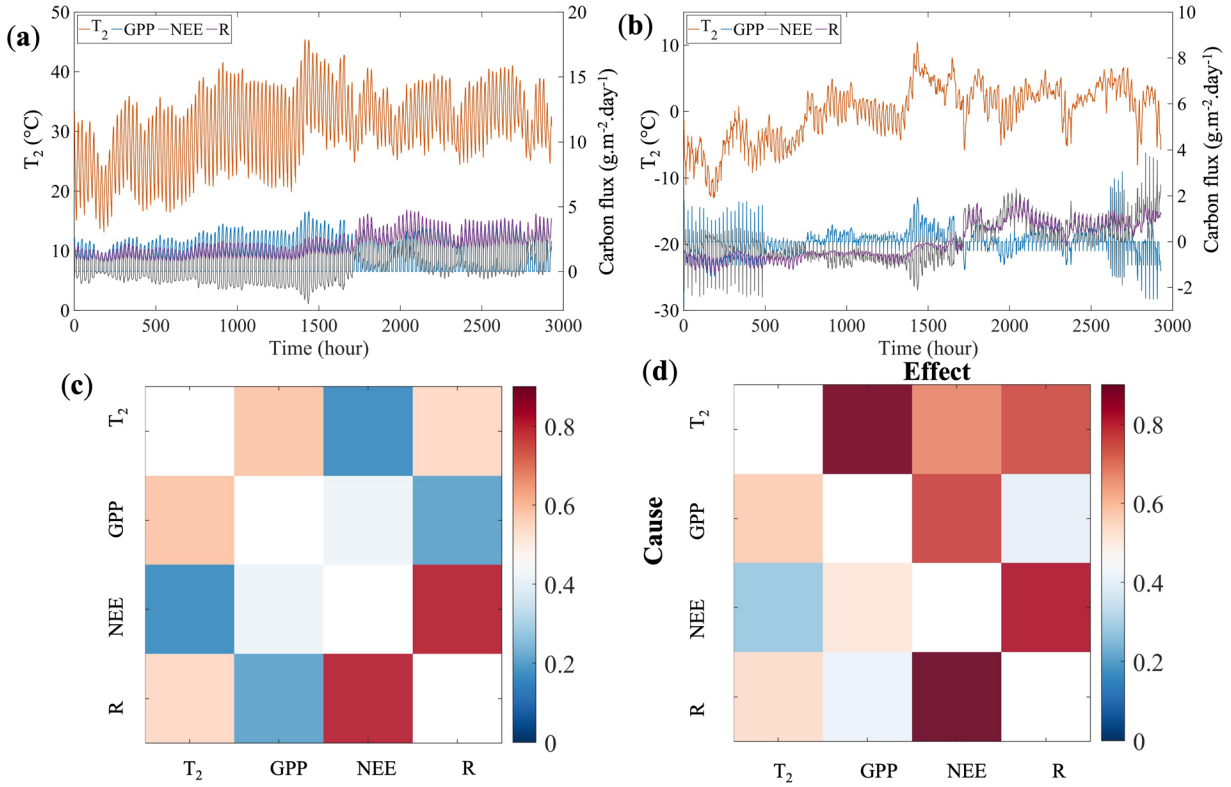


**Figure 3.** WRF-generated data (a) hourly time series of  $T_2$ , GPP, NEE, and R in the summer of 2013 and (b) anomalies after detrending, for the quantification and comparisons of heat-carbon coupling strength using (c) the statistical correlation coefficient, and (d) the CCM method.

### 3.3. The impact of urban irrigation on heat-carbon feedback

We then extended the CCM analysis to all urban areas in CONUS, using the four key outputs by WRF. We first focused on the *local* impact of urban irrigation on the heat-carbon coupling, viz. the change of causality strength due to irrigation measured by the difference between the irrigated and the baseline scenarios  $\Delta\rho_{X|M_Y} = \rho_{X|M_Y, \text{irrigated}} - \rho_{X|M_Y, \text{no-irrigation}}$ , with  $\rho_{X|M_Y}$  defined in Eq. (3). By *local*, we mean the difference is taken at same urban area, e.g. Phoenix

city, without considering the potential causal influence among temperature and carbon fluxes to or from another urban pixel, be it adjacent or distant. The results of all  $\Delta\rho_{X|M_Y}$ , with the generic variables  $X$  and  $Y$  representing  $T_2$ , R, GPP, and NEE alternatively, are shown in **Fig. 4** mapped onto all urban areas in CONUS. The color bars represent the difference in the *magnitude* of  $\Delta\rho_{X|M_Y}$ , instead of *fractional* changes. The reason of avoiding the use of fractional changes is that fractional changes can give rise to a false significance in the change when the coupling is weak, e.g. an increase of  $\rho_{X|M_Y}$  from 0.01 to 0.02 stands for 100% of change, yet both are insignificant in terms of coupling strength.

The results show that the most significant local impact of urban irrigation occurs in the west CONUS between  $T_2$  and R (the first row of Fig. 4), where the coupling of temperature and soil respiration is significantly strengthened, especially in metropolitan areas in the states of Texas, California, and Washington. It is not a coincidence that this change is in good agreement with the WRF simulation results in the areas where urban irrigation enhances soil respiration, i.e. the trade-off regions for heat-carbon mitigations. In contrast, in the east CONUS that marks the co-benefit of heat-carbon mitigation, viz. both temperature and soil respiration are reduced by urban irrigation, the strength of  $T_2$ -R coupling remains largely the same or weakly decreases. The impact of urban irrigation on  $T_2$ -R coupling is bi-directional, as revealed by the similarity of spatial distribution in Fig. 4a and Fig. 4b.

The impact of urban irrigation on  $T_2$ -GPP coupling (Fig. 4c and 4d) is much less significant as compared to that on the  $T_2$ -R counterpart. We can only trace a mildly enhanced coupling trend along the coastal cities in the south (Florida, Texas, and South California), whereas the  $T_2$ -GPP coupling in most of the inland urban areas remains largely indifferent to irrigation. The resultant  $T_2$ -NEE coupling, resultant in the sense that NEE is determined as the sum of R and GPP,

exhibits mixed and complex patterns in its response to urban irrigation (Fig. 4e and 4f), due to the complex and highly nonlinear pathway governing the interactions between urban ambient temperature and the net ecosystem exchange (Yuan et al., 2011).

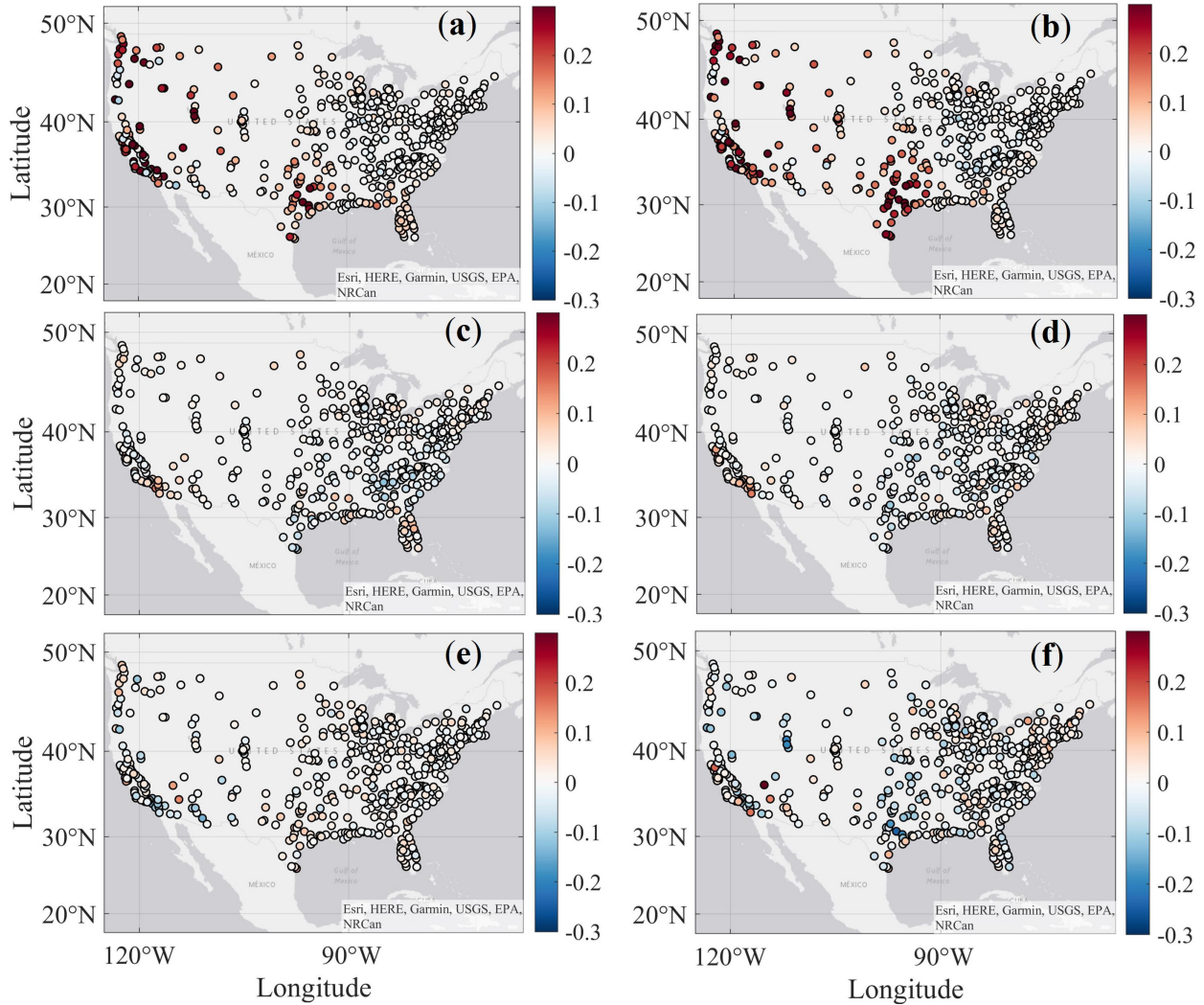


**Figure 4.** The results of *local* difference of causality strength on heat-carbon coupling between the irrigated and baseline scenarios, for (a)  $\Delta\rho_{T_2|M_R}$ , (c)  $\Delta\rho_{T_2|M_{GPP}}$ , (e)  $\Delta\rho_{T_2|M_{NEE}}$  from temperature to carbon fluxes, and (b)  $\Delta\rho_{M_R|T_2}$ , (d)  $\Delta\rho_{M_{GPP}|T_2}$ , (f)  $\Delta\rho_{M_{NEE}|T_2}$  from carbon fluxes to temperature, respectively.

Lastly, we proceeded to look into the *non-local* impact of urban irrigation on heat-carbon interactions. In this case, the changes of causality strength in a given city, giving rise to or resulted from all other urban areas (except itself, which is considered as the local impact as discussed above), need to be considered. To quantify the outgoing (causal influence) and incoming (causal susceptibility) influence at the locality, we therefore use the average causal effect (ACE) and the average causal susceptibility (ACS) at a given city with an index  $i$ , defined by (Runge et al., 2015)

$$\text{ACE}_i = \frac{1}{n-1} \sum_{j \neq i} \rho_{X_i | M_{Y,j}}, \quad (4)$$

$$\text{ACS}_i = \frac{1}{n-1} \sum_{j \neq i} \rho_{X_j | M_{Y,i}}, \quad (5)$$

where  $n$  is the total number of CONUS cities. Mathematically, ACE and ACS represent the averages over columns and rows of the  $n \times n$  causality matrix, respectively, over the spatially mapping of all CONUS cities.

The results of irrigation-induced non-local changes in ACE are shown in **Fig. 5**. The results of ACS exhibit similar patterns reciprocal to its counterpart of ACE and are therefore not shown. The first thing to be noticed is that the non-local impact of urban irrigation is almost negligible everywhere over the entire CONUS, except that the ACE from R to  $T_2$  (**Fig. 5b**). The non-local ACE change from R to  $T_2$  can be interpreted as the causal effect (influence) exerted by the local change of soil respiration on non-local ambient temperatures *averaged over all other* CONUS cities via the application of urban irrigation. The results of ACS (not shown here) reveal, on the other hand, a manifest *reciprocal causal susceptibility* of local urban temperature to the change of respiration induced by irrigation aggregated over other cities. The impact is *far-reaching* as

compared to the local effect (in Fig. 4), as it implies there exists potentially long-range impact (viz. the *teleconnection*) of urban irrigation in influencing the built environment at long distance (de Vrese et al., 2016). In our case, the teleconnection is discerned in the interaction between  $T_2$  and R, with urban irrigation has the potential to enhance the heat-carbon (in this case, R) coupling in most of the west CONUS cities, but weaken the causal feedback in south California cities.

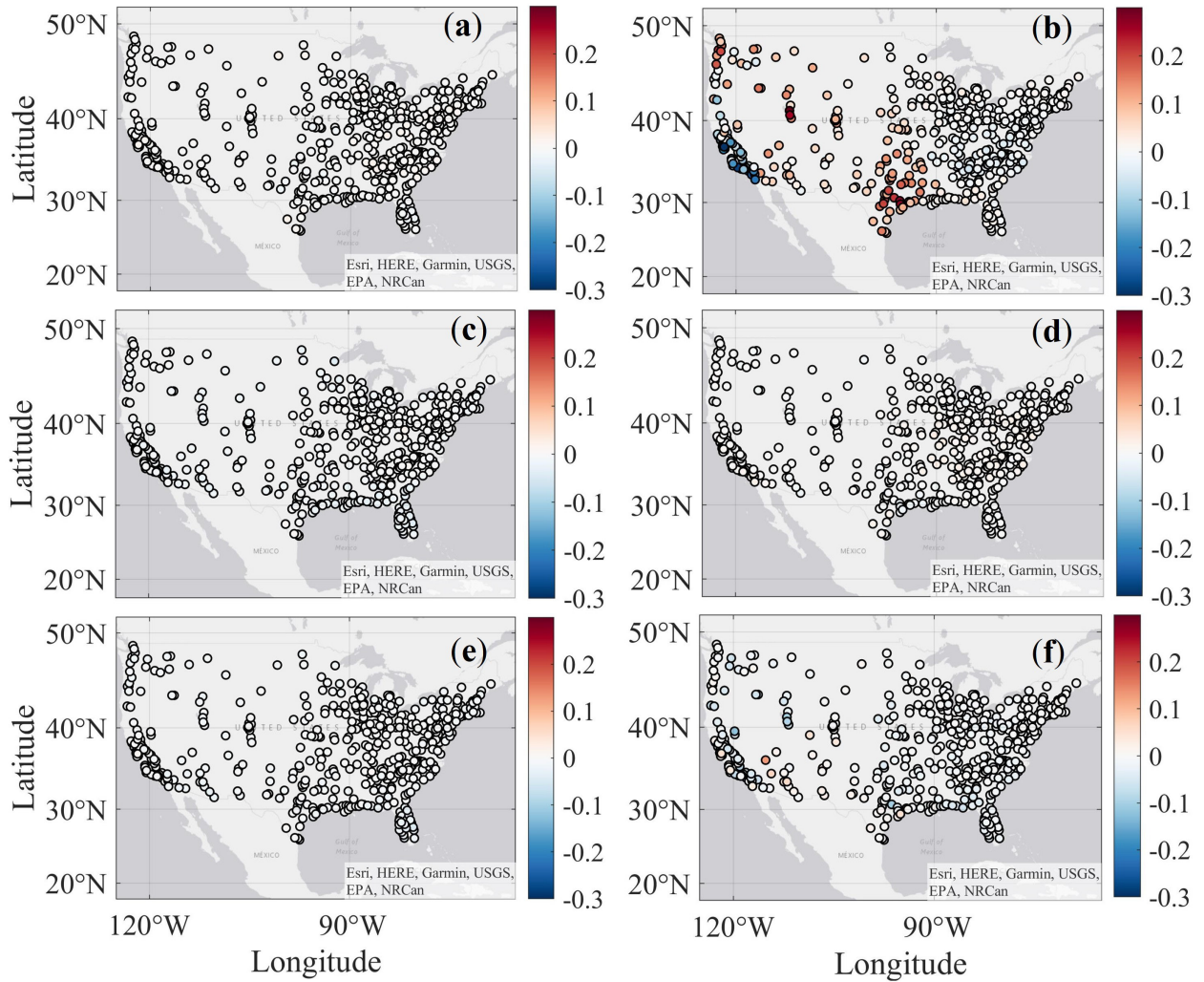


**Figure 5.** The results of *non-local* impact of urban irrigation on ACE of heat-carbon coupling between the irrigated and baseline scenarios, for (a)  $T_2$  to R, (c)  $T_2$  to GPP, (e)  $T_2$  to NEE, and (b) R to  $T_2$ , (d) GPP to  $T_2$ , (f) NEE to  $T_2$ , respectively.

## 4. Concluding Remarks

In this study, we quantified the impact of urban irrigation on the strength of coupling between ambient temperature and surface exchange of CO<sub>2</sub> fluxes via, soil respiration, carbon assimilation by vegetation, and the resultant net ecosystem exchange. We find that the application of urban irrigation in CONUS cities causes a ubiquitous cooling effect, but its impact on carbon fluxes via complex interplay of heat-carbon dynamics is far more complicated and intriguing. In general, the net effect is an environmental *co-benefit* of both heat and carbon mitigation in the east half of CONUS, but a manifest *trade-off* in the west via enhanced soil respiration (abiotic carbon emission). The local impact of urban irrigation on heat-carbon coupling, with soil respiration as the dominant carbon exchange process in urban areas, follows a similar spatial distribution, viz. a strengthening of coupling strength and potential feedback mechanisms in the west, weakening in the east. The non-local effect only exists between the causal influence exerted on ambient temperature by soil respiration in the west U.S., signaling a far-reaching impact of potential teleconnection of urban irrigation.

It is caveated that the measure of heat-carbon feedback mechanisms we adopted in this study, viz. the causality strength quantified by the CCM method, is by no means unique. Rather, the proposed method should be viewed as experimental in nature. There are other valid, or even better, methods to unravel the complex interplay of heat and carbon dynamics in urban areas, such as Granger or Bayesian causal inference. Yet, in the light of this pioneering work, the CCM method is a good candidate for such a task, especially given that urban surface processes constitute a highly nonlinear dynamic system with all the environmental variables (e.g. temperature, soil moisture, humidity, and scalar transport) subtly and intrinsically connected. While we focused on four key variables in this study, the coupling among different variables

may exhibit very different or more complex (c.f. temperature and NEE) behavior, locally and non-locally. Their distinctive patterns of interactions will have important and far-reaching implications for relevant stakeholders, e.g. urban planners, practitioners, environmental managers, and policymakers, to seek sustainable solutions to mitigate the adverse environmental impact and promoting overall liveability of urban areas, especially mega-cities, among which urban irrigation is but one singular, though undoubtedly very important, strategy. For example, given the potential long-range impact of irrigation on the heat and carbon dynamics of some remote urban areas, stakeholders from different cities/regions should cooperate more closely to optimize urban mitigation/adaptation strategies via better coordinated and synergistic means.

## **Acknowledgement**

This study is supported by the U. S. National Science Foundation (NSF) under Grant number CBET-2028868, the National Aeronautics and Space Administration (NASA) under grant # 80NSSC20K1263, and Arizona Board of Regents (ABOR) through the project “Smart Tree Watering in Arizona’s Urban Environment”.

## References:

- Antognelli, S., & Vizzari, M. (2016). Ecosystem and urban services for landscape liveability: A model for quantification of stakeholders' perceived importance. *Land Use Policy*, *50*, 277-292.
- Chen, F., Kusaka, H., Bornstein, R., Ching, J., Grimmond, C.S.B., Grossman-Clarke, S., Loridan, T., Manning, K.W., Martilli, A., Miao, S.G., Sailor, D., Salamanca, F.P., Taha, H., Tewari, M., Wang, X.M., Wyszogrodzki, A.A., & Zhang, C.L. (2011). The integrated WRF/urban modelling system: development, evaluation, and applications to urban environmental problems. *International Journal of Climatology*, *31*(2), 273-288.
- de Vrese, P., Hagemann, S., & Claussen, M. (2016). Asian irrigation, African rain: Remote impacts of irrigation. *Geophysical Research Letters*, *43*, 3737-3745.
- Decina, S. M., Hutryra, L. R., Gately, C. K., Getson, J. M., Reinmann, A. B., Short Gianotti, A. G., et al. (2016), Soil respiration contributes substantially to urban carbon fluxes in the greater Boston area, *Environmental Pollution*, *212*, 433-439.
- Demetillo, M.A.G., Navarro, A., Knowles, K.K., Fields, K.P., Geddes, J.A., Nowlan, C.R., Janz, S.J., Judd, L.M., Al-Saadi, J., Sun, K., McDonald, B.C., Diskin, G.S., & Pusede, S.E. (2020). Observing nitrogen dioxide air pollution inequality using high-spatial-resolution remote sensing measurements in Houston, Texas. *Environmental Science & Technology*, *54*(16), 9882-9895.
- Fernando, H.J.S. (2010). Fluid dynamics of urban atmospheres in complex terrain. *Annual Review of Fluid Mechanics*, *42*, 365-389.
- Fitzpatrick, M.C., & Dunn, R.R. (2019). Contemporary climatic analogs for 540 North American urban areas in the late 21st century. *Nature Communications*, *10*, 614-617.

- Gao, J., & O'Neill, B.C. (2020). Mapping global urban land for the 21st century with data-driven simulations and Shared Socioeconomic Pathways. *Nature Communications*, *11*(1), 2302.
- Gober, P., Brazel, A., Quay, R., Myint, S., Grossman-Clarke, S., Miller, A., & Rossi, S. (2010). Using watered landscapes to manipulate urban heat island effects: How much water will it take to cool Phoenix? *Journal of the American Planning Association*, *76*(1), 109-121.
- Grassberger, P., & Procaccia, I. (1983). Characterization of strange attractors. *Physical Review Letters*, *50*(5), 346-349.
- Gurney, K.R. (2014). Recent research quantifying anthropogenic CO<sub>2</sub> emissions at the street scale within the urban domain. *Carbon Management*, *5*(3), 309-320.
- Habeeb, D., Vargo, J., & Stone, B. (2015). Rising heat wave trends in large US cities. *Natural Hazards*, *76*(3), 1651-1665.
- Hardiman, B. S., Wang, J. A., Hutyra, L. R., Gately, C. K., Getson, J. M., & Friedl, M. A. (2017). Accounting for urban biogenic fluxes in regional carbon budgets, *Science of the Total Environment*, *592*, 366-372.
- Huovila, A., Siikavirta, H., Antuña Rozado, C., Rökman, J., Tuominen, P., Paiho, S., Hedman, Å., & Ylén, P. (2022). Carbon-neutral cities: Critical review of theory and practice. *Journal of Cleaner Production*, *341*, 130912.
- Hutyra, L.R., Duren, R., Gurney, K.R., Grimm, N., Kort, E.A., Larson, E., & Shrestha, G. (2014). Urbanization and the carbon cycle: Current capabilities and research outlook from the natural sciences perspective. *Earth's Future*, *2*(10), 473-495.
- IPCC (2022), Climate Change 2022: Impact, Adaptation and Vulnerability. Summary for Policymakers, 37 pp, Intergovernmental Panel on Climate Change.
- Kindler, M., Vivoni, E. R., Pérez-Ruiz, E. R., & Wang, Z. (2022), Water conservation potential

of modified turf grass irrigation in urban parks of Phoenix, Arizona, *Ecohydrology*, 15(3), e2399.

Kumar, P., Druckman, A., Gallagher, J., Gatersleben, B., Allison, S., Eisenman, T.S., Hoang, U., Hama, S., Tiwari, A., Sharma, A., Abhijith, K.V., Adlakha, D., McNabola, A., Astell-Burt, T., Feng, X., Skeldon, A.C., de Lusignan, S., & Morawska, L. (2019). The nexus between air pollution, green infrastructure and human health. *Environment International*, 133, 105181.

Lai, Y.-C., & Ye, N. (2003). Recent developments in chaotic time series analysis. *International Journal of Bifurcation and Chaos*, 13(06), 1383-1422.

Lambin, E.F., & Meyfroidt, P. (2011). Global land use change, economic globalization, and the looming land scarcity. *Proceedings of the National Academy of Sciences of the United States of America*, 108(9), 3465-3472.

Li, P., & Wang, Z. H. (2020). Modeling carbon dioxide exchange in a single-layer urban canopy model. *Building and Environment*, 184, 107243.

Li, P., & Wang, Z.H. (2021a). Environmental co-benefits of urban greening for mitigating heat and carbon emissions. *Journal of Environmental Management*, 293, 112963.

Li, P., & Wang, Z.H. (2021b). Uncertainty and sensitivity analysis of modeling plant CO<sub>2</sub> exchange in the built environment. *Building and Environment*, 189, 107539.

Li, P., Xu, T., Wei, S., & Wang, Z.H. (2022). Multi-objective optimization of urban environmental system design using machine learning. *Computers, Environment and Urban Systems*, 94, 101796.

Luketich, A.M., Papuga, S.A., & Crimmins, M.A. (2019). Ecohydrology of urban trees under passive and active irrigation in a semiarid city. *PLoS One*, 14(11), e0224804.

- Mysterud, A., Stenseth, N. C., Yoccoz, N. G., Langvatn, R., & Steinheim, G. (2001), Nonlinear effects of large-scale climatic variability on wild and domestic herbivores, *Nature*, 410(6832), 1096-1099.
- Niu, G.Y., Yang, Z.L., Mitchell, K.E., Chen, F., Ek, M.B., Barlage, M., Kumar, A., Manning, K., Niyogi, D., Rosero, E., Tewari, M., & Xia, Y.L. (2011). The community Noah land surface model with multiparameterization options (Noah-MP): 1. Model description and evaluation with local-scale measurements. *Journal of Geophysical Research-Atmospheres*, 116, D12109.
- Oke, T.R. (1967). City size and the urban heat island. *Atmospheric Environment*, 7, 769-779.
- Oke, T.R. (1982). The energetic basis of the urban heat island. *Quarterly Journal of the Royal Meteorological Society*, 108(455), 1-24.
- Pataki, D.E., Bowling, D.R., Ehleringer, J.R., & Zobitz, J.M. (2006). High resolution atmospheric monitoring of urban carbon dioxide sources. *Geophysical Research Letters*, 33(3), L03813.
- Pearl, J., & Mackenzie, D. (2018), *The Book of Why: The New Science of Cause and Effect*, Basic Books, 432 pp.
- Randerson, J.T., Lindsay, K., Munoz, E., Fu, W., Moore, J.K., Hoffman, F.M., Mahowald, N.M., & Doney, S.C. (2015). Multicentury changes in ocean and land contributions to the climate-carbon feedback. *Global Biogeochemical Cycles*, 29(6), 744-759.
- Ronda, R. J., de Bruin, H. A. R., & Holtslag, A. A. M. (2001), Representation of the canopy conductance in modeling the surface energy budget for low vegetation, *Journal of Applied Meteorology*, 40(8), 1431-1444.
- Runge, J., Bathiany, S., Bollt, E., Camps-Valls, G., Coumou, D., Deyle, E., et al. (2019),

- Inferring causation from time series in Earth system sciences, *Nature Communications*, 10, 2553.
- Runge, J., Petoukhov, V., Donges, J. F., Hlinka, J., Jajcay, N., Vejmelka, M., et al. (2015), Identifying causal gateways and mediators in complex spatio-temporal systems, *Nature Communications*, 6, 8502.
- Sargent, M., Barrera, Y., Nehrkorn, T., Hutyra, L. R., Gately, C. K., Jones, T., et al. (2018), Anthropogenic and biogenic CO<sub>2</sub> fluxes in the Boston urban region, *Proceedings of the National Academy of Sciences of the United States of America*, 115(29), 7491-7496.
- Seto, K.C., Fragkias, M., Guneralp, B., & Reilly, M.K. (2011). A meta-analysis of global urban land expansion. *PLoS One*, 6(8), e23777.
- Seto, K.C., Reenberg, A., Boone, C.G., Fragkias, M., Haase, D., Langanke, T., Marcotullio, P., Munroe, D.K., Olah, B., & Simon, D. (2012). Urban land teleconnections and sustainability. *Proceedings of the National Academy of Sciences of the United States of America*, 109(20), 7687-7692.
- Skamarock, W. C., Klemp, J. B., Dudhia, J., Gill, D. O., Liu, Z., Berner, J., et al. (2019), A Description of the Advanced Research WRF Model Version 4.3, Report #NCAR/TN-556+STR, National Center for Atmospheric Research, Boulder, USA, 165 pp.
- Song, J., & Wang, Z. H. (2015), Interfacing urban land-atmosphere through coupled urban canopy and atmospheric models, *Boundary-Layer Meteorology*, 154(3), 427-448.
- Song, J., & Wang, Z. H. (2016), Evaluating the impact of built environment characteristics on urban boundary layer dynamics using an advanced stochastic approach, *Atmospheric Chemistry and Physics*, 16, 6285-6301.
- Song, J., Wang, Z. H., & Wang, C. (2017), Biospheric and anthropogenic contributors to

- atmospheric CO<sub>2</sub> variability in a residential neighborhood of Phoenix, Arizona, *Journal of Geophysical Research: Atmospheres*, 122, 3317-3329.
- Sugihara, G., May, R., Ye, H., Hsieh, C.H., Deyle, E., Fogarty, M., & Munch, S. (2012). Detecting causality in complex ecosystems. *Science*, 338(6106), 496-500.
- Sugihara, G., & May, R.M. (1990). Nonlinear forecasting as a way of distinguishing chaos from measurement error in time series. *Nature*, 344(6268), 734-741.
- Takens, F. (1981), Detecting strange attractors in fluid turbulence, in dynamical systems and turbulence, edited by D. Rand and L. S. Young, pp. 366-381, Springer-Verlag, Berlin.
- UN-Habitat (2020), World Cities Report 2020: The Value of Sustainable Urbanization, 377 pp, United Nations Human Settlements Programme, Nairobi, Kenya.
- United Nations (UN) (2019), World Urbanization Prospects: The 2018 Revision, 126 pp, The United Nations' Department of Economic and Social Affairs - Population Division, New York.
- USGCRP (2016), The Impacts of Climate Change on Human Health in the United States: A Scientific Assessment, 312 pp, U.S. Global Change Research Program, Washington, DC.
- Wang, C., Wang, Z.H., & Yang, J. (2018). Cooling effect of urban trees on the built environment of contiguous United States. *Earth's Future*, 6, 1066-1081.
- Wang, C., Wang, Z.H., & Yang, J. (2019a). Urban water capacity: Irrigation for heat mitigation. *Computers, Environment and Urban Systems*, 78, 101397.
- Wang, C., Wang, Z.H., Wang, C., & Myint, S.W. (2019b). Environmental cooling provided by urban trees under extreme heat and cold waves. *Remote Sensing of Environment*, 227, 28-43.
- Wang, C., Wang, Z. H., & Ryu, Y. H. (2021). A single-layer urban canopy model with

- transmissive radiation exchange between trees and street canyons. *Building and Environment*, 191, 107593.
- Wang, Z.H. (2021). Compound environmental impact of urban mitigation strategies: Co-benefits, trade-offs, and unintended consequence. *Sustainable Cities and Society*, 75, 103284.
- Wang, Z.H. (2022). Reconceptualizing urban heat island: Beyond the urban-rural dichotomy. *Sustainable Cities and Society*, 77, 103581.
- Wang, Z. H., Bou-Zeid, E., & Smith, J. A. (2013), A coupled energy transport and hydrological model for urban canopies evaluated using a wireless sensor network, *Quarterly Journal of the Royal Meteorological Society*, 139(675), 1643-1657.
- Wang, Z.H., & Upreti, R. (2019). A scenario analysis of thermal environmental changes induced by urban growth in Colorado River Basin, USA. *Landscape and Urban Planning*, 181, 125-138.
- Wickham, J., Homer, C., Vogelmann, J., McKerrow, A., Mueller, R., Herold, N., & Coulston, J. (2014). The multi-resolution land characteristics (MRLC) consortium - 20 years of development and integration of USA National Land Cover Data. *Remote Sensing*, 6(8), 7424-7441.
- Yang, J., & Wang, Z.H. (2015). Optimizing urban irrigation schemes for the trade-off between energy and water consumption. *Energy and Buildings*, 107, 335-344.
- Yang, X., Wang, Z.H., Wang, C., & Lai, Y.C. (2022). Detecting the causal influence of thermal environments among climate regions in the United States. *Journal of Environmental Management*, 116001.
- Yang, X., Wang, Z. H., Wang, C., & Lai, Y.C. (2023). Finding causal gateways of precipitation

over the contiguous United States. *Geophysical Research Letters*, 50(4), e2022GL101942.

Yuan, W., Luo, Y., Liang, S., Yu, G., Niu, S., Stoy, P., et al. (2011), Thermal adaptation of net ecosystem exchange, *Biogeosciences*, 8(6), 1453-1463.